

Elastic Scattering Events at HERMES

Cory Schillaci

Date: September 16, 2008

Supervisors: Sergey Yaschenko, Achim Hillenbrand

Contents

1	Introduction	1
1.1	HERMES Spectrometer and Recoil Detector	1
1.1.1	The Forward Spectrometer	1
1.1.2	The Recoil Detector	2
1.2	Motivation and Goals	3
2	Elastic Event Selection	3
2.1	Scattered Beam Lepton Selection	4
2.2	Scattered Proton Selection	5
2.3	Lepton-Proton Correlation Cuts	5
2.3.1	Correlation of ϕ Angles	6
2.3.2	Correlation of Calculated and Measured θ Angles for the Proton	6
2.3.3	Correlation of Z-Vertex Values	6
2.3.4	Effects of Correlation Cuts	7
3	Elastic and Quasi-Elastic Scattering on Deuteron Target	8
4	Detector Alignment and Efficiency	9
4.1	θ and ϕ Acceptance	9
4.2	Z-vertex Misalignment	11
4.3	Momentum Measurements	11
4.4	Q^2 Distribution	13
5	Summary and Outlook	15

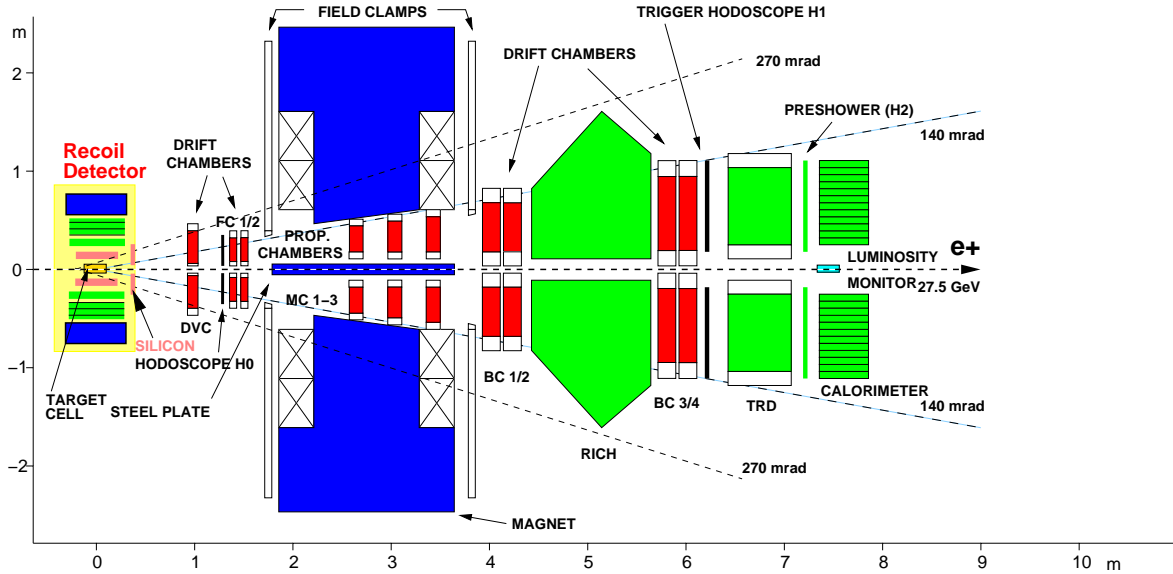


Figure 1.1: Diagram of the HERMES Spectrometer

1 Introduction

1.1 HERMES Spectrometer and Recoil Detector

The HERA Measurement of Nucleon Spin (HERMES) experiment was designed to study the source of the proton spin. Originally, the experiment consisted of a stationary target of polarized gas and a spectrometer in the scattering direction (called the Forward Spectrometer). In 2006, the Recoil Detector was added, surrounding the target, to detect particles at large angles and low energies. An unpolarized gas target was also installed at this time. See Figure 1.1 for a schematic.

1.1.1 The Forward Spectrometer

The HERMES Forward Spectrometer is shown on the right part of Figure 1.1. As specific details of Forward Spectrometer components are not addressed in this report, only a summary of the various detectors is given below.

- Vertex Chambers (VC 1/2): tracking system using microstrip gas chambers
- Drift Vertex Chambers (DVC): increases the redundancy of tracking system
- Front Chambers (FC 1/2): drift chambers
- Magnet Chambers (MC 1-3): multiwire proportional chambers for momentum analysis of relatively low energy particles

- Back Chambers (BC 1-4): drift chambers
- Dual-Radiator Ring Image Čerenkov Counter (RICH): allows separation of pions, kaons and protons
- Transition Radiation Detector (TRD): distinguishes between electrons and hadrons
- Calorimeter: measures the energy of the particles
- Hodoscope: composed of scintillators, discriminates between electrons and hadrons
- Moun Wall: one meter deep iron wall to decelerate mouns for detection by the Muon Hodoscopes behind the wall

1.1.2 The Recoil Detector

The Recoil Detector consists of three sensor systems surrounded by a magnet which produces a 1.0T magnetic field in the longitudinal beam direction. The innermost detector system is the Silicon Strip Detector (SSD), arranged in a four-sided diamond pattern. The SSD contains two modules, the Inner SSD and Outer SSD, and each module consists of two perpendicular layers of silicon strips. Outside of the SSD is the Scintillating Fiber Tracker (SFT). There are two cylinders in the SFT, each composed of four layers of scintillating fibers. Of the four layers per cylinder, two are parallel to the beam axis and two are at a stereo angle of 10° . The outermost detector is the Photon Detector (PD), consisting of alternating layers of tungsten and scintillator strips.

Combination of the two SSD modules and the two SFT cylinders gives a total of four tracking layers for charged particles. A particle's momentum is reconstructed from the curvature of its path through these detectors in the magnetic field. Data from the PD is not used in analysis of elastic events, as no photon is produced.

Four quadrants of the Recoil Detector are defined by the four sides of the SSD, numbered as follows (ϕ angles are defined as if facing the detector from the incoming beam direction):

- Quadrant 1: $3\pi/2 < \phi < 2\pi$
- Quadrant 2: $0 < \phi < \pi/2$
- Quadrant 3: $\pi/2 < \phi < \pi$
- Quadrant 4: $\pi < \phi < 3\pi/2$

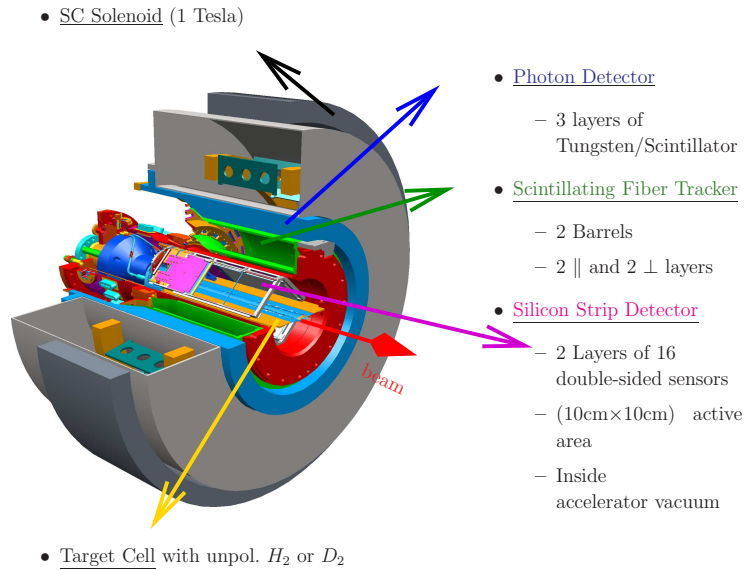


Figure 1.2: Diagram of the HERMES Recoil Detector

1.2 Motivation and Goals

It was originally hoped that an absolute cross section for the scattering events could be calculated. Elastic cross sections can be used to determine proton elastic form factors [1]. At this time, however, detector efficiency and luminosity are not sufficiently understood for the calculation of absolute cross sections.

Instead, the project focused more on the detector itself. Because elastic scattering is simple and well understood, data from these events can be used to evaluate detector alignment. These elastically scattered protons have much higher momenta (1-3 GeV/c) than the particles in the normal operating range of the Recoil Detector, and can therefore be used to evaluate an extreme regime of the detector. A search for elastic deuteron scattering was also attempted as a way to detect possible contamination of the target with heavy nucleons.

2 Elastic Event Selection

The selection of elastic events is divided into three steps. First, data corresponding to the elastically scattered beam lepton is identified. The elastically scattered proton is then identified. Finally, cuts are made on expected correlations between the two outgoing particles in order to significantly reduce background.

2.1 Scattered Beam Lepton Selection

The scattered beam lepton is selected based on momentum, charge and Particle Identification Value (PID). Incoming beam leptons are assumed to have a momentum of 27.57 GeV/c. A scattered lepton is required to have a reconstructed momentum between 25 GeV/c and 30 GeV/c.

For particle identification, the PID1 value is used. PID values are calculated as the log of the ratio of probabilities for leptons and hadrons (Equation 2.1). The PID1 value is required to be greater than zero for a track to qualify as a lepton. PID1 includes particle identification from the preshower only. Use of PID2+5 (the sum of PID values from the preshower, TRD, and calorimeter) was originally tried, but found to exclude an unreasonably large number of events. See Figure 2.1 for distributions of the various PID values. Further investigation is necessary regarding the unexpected behavior in the PID distributions. Cuts on the pulses in the TRD and Preshower are used as additional rough approximations to PID requirements. TRD pulses between 16 and 100 KeV and Preshower pulses between 10^{-2} and 10^5 MeV were selected.

$$\text{PID} = \log_{10}\left(\frac{P_{\text{lepton}}(E, p, \dots)}{P_{\text{hadron}}(E, p, \dots)}\right) \quad (2.1)$$

A check is also made that the sign of the charge matches the sign of the incoming lepton's charge. Only positron data from 2007 was used, so the lepton was always required to be positively charged.

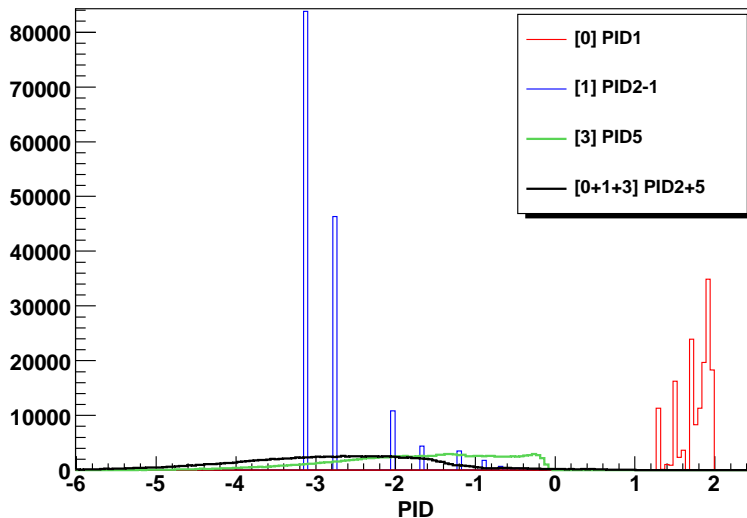


Figure 2.1: Plot of different PID values from PIDlib and the sum. The numbers in the bracket correspond to the array index as returned by PIDlib. [0] is from the Preshower, [1] is from the Calorimeter, and [3] is from the TRD.

	ϕ Diff [rad]		θ Diff [mrad]		Z Diff [cm]	
	Mean	σ	Mean	σ	Mean	σ
Quadrant 1	3.145	.009973	56.56	14.91	.1488	.8458
Quadrant 2	-3.151	.009363	19.15	13.53	1.048	.7501
Quadrant 3	-3.144	.008522	24.51	11.49	.0649	.8455
Quadrant 4	3.144	.008741	42.68	12.76	-1.159	.736
Monte Carlo (Q1)	3.136	.007883	14.15	8.855	-0.1	1.095

Table 2.1: Numbers used for the correlation cuts. Monte Carlo data from Quadrant 1 is also given for comparison.

2.2 Scattered Proton Selection

A scattered proton is identified simply as the track in the Recoil Detector with the highest momentum. The cuts described in Sections 2.3 and 2.1 are thought to be sufficient to select elastic events. Two requirements were initially imposed, but later thrown out.

First, the Recoil Detector was required to have registered at least four space points, one in each of the following: Inner SSD, Outer SSD, Inner SFT, and Outer SFT. This cut is not feasible due to inefficiency; it reduced the statistics by a factor of approximately four in Quadrants 2-4 and a factor of about ten in Quadrant 1.

Second, the event was discarded if more than one particle was identified in the Recoil Detector which met the four space point requirement. Allowing multiple tracks improves the number of data points and is more reasonable when only three space points are required for the proton track.

2.3 Lepton-Proton Correlation Cuts

In order to reduce background and improve data, a study was made of the correlations between certain variables for the lepton in the Forward Spectrometer and the proton in the Recoil Detector. Cuts were made separately on individual quadrants for each type of correlation. A gaussian fit was used on each peak. All events within three σ of the mean are included in the final analysis. See Table 2.1 for the relevant numerical data for each cut. Calculations are made using 27.57 GeV/c for the incident beam lepton momentum.

2.3.1 Correlation of ϕ Angles

The azimuthal angle, ϕ of the particles is ideally expected to differ by π due to momentum conservation. A strong correlation is therefore expected. Plots of the difference are made by quadrant of the Recoil Detector, and demonstrate the expected correlation along with background. See Figure 2.2 for an example.

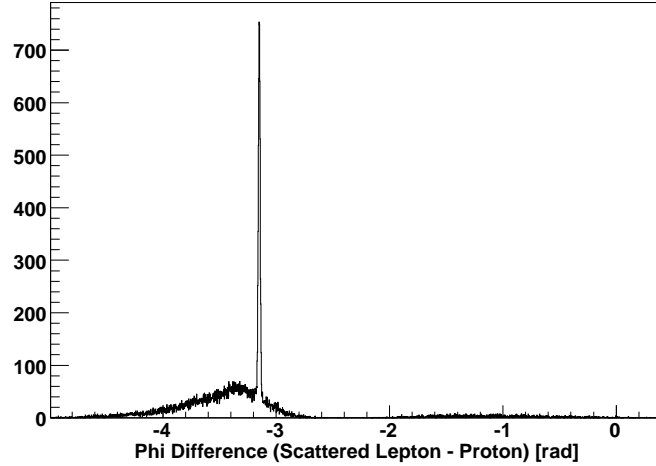


Figure 2.2: Correlation and background of the ϕ difference (lepton-proton) for events in which the proton was detected in Quadrant 3 of the Recoil Detector.

2.3.2 Correlation of Calculated and Measured θ Angles for the Proton

The polar angle θ is also expected to be correlated between the two particles. Because the kinematics of the two body collision are entirely determined by the incoming beam momentum and θ of the scattered lepton, the expected proton θ angle can be calculated. An analysis is made of the relationship between the actual θ angle measured for the proton in the Recoil Detector and the expected proton θ calculated from the θ angle of the beam lepton in the Forward Spectrometer. See Figure 2.3.

2.3.3 Correlation of Z-Vertex Values

The Z position of the event vertex should be identical for the two particles from an elastic event. The distribution of the differences in measured Z-vertex values is therefore used to define another cut. Studies of the correlation after the selection in sections 2.1 and 2.2 show a much lower apparent background than in the ϕ and θ distributions. Figure 2.4 shows that most of the events fall within the three σ cut. These cuts

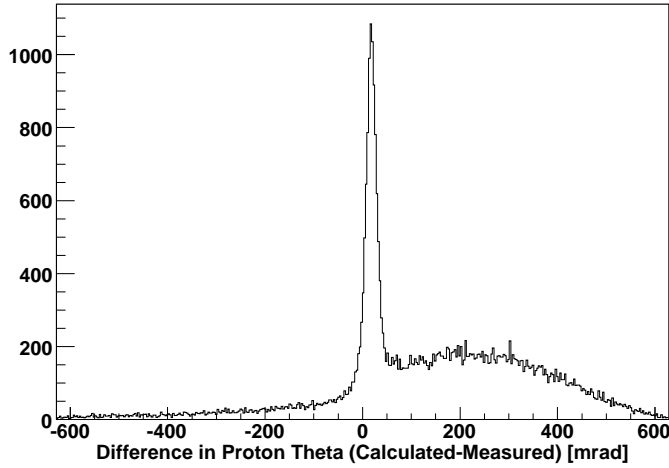


Figure 2.3: Correlation and background of the θ difference (calculated-measured) for events in which the proton was detected in Quadrant 2 of the Recoil Detector.

were therefore less useful in reducing the remaining background events, but were still implemented.

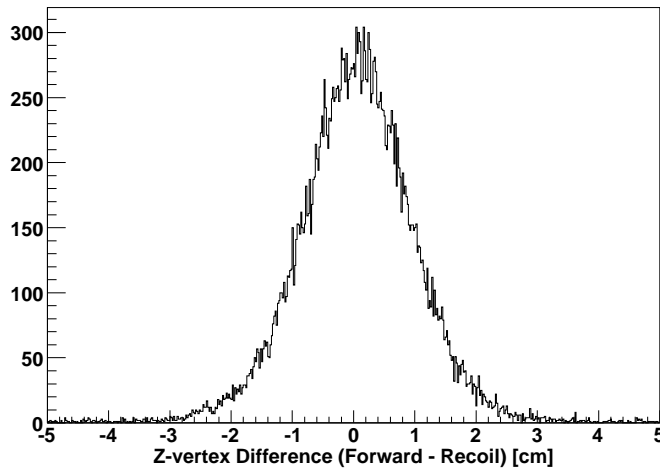


Figure 2.4: Correlation and background of the event Z-vertex as measured in the Forward Spectrometer and Recoil Detector for events in which the proton was detected in Quadrant 3 of the Recoil Detector.

2.3.4 Effects of Correlation Cuts

Evidence of the effectiveness of the cuts can be seen in Figure 2.5. The measured momentum of the proton is much better correlated with that expected in an elastic event (calculated from lepton θ) after the correlation cuts.

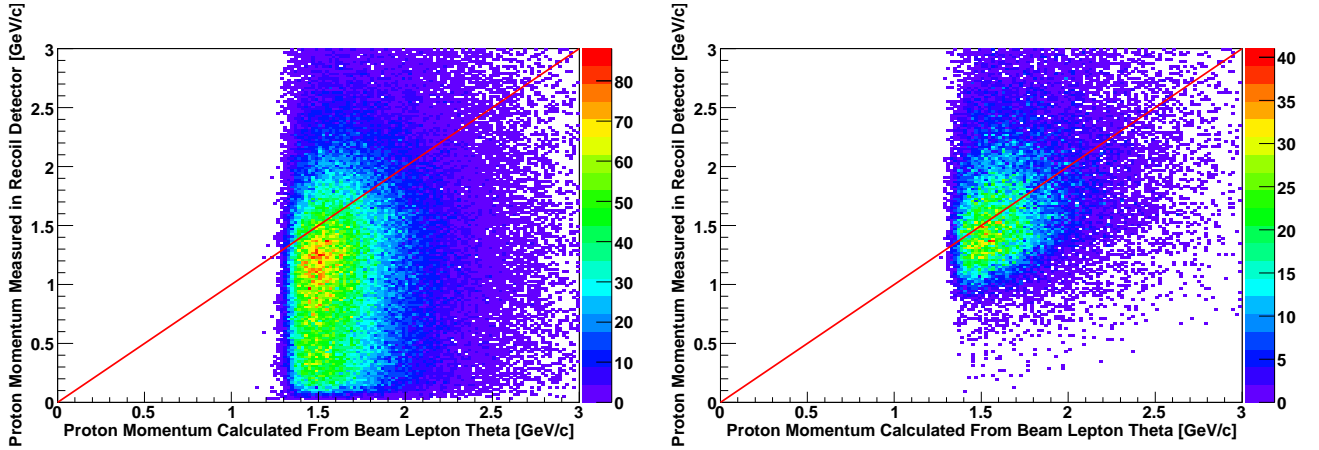


Figure 2.5: Correlation of the measured and calculated momentum of the proton before (left) and after (right) the correlation cuts.

3 Elastic and Quasi-Elastic Scattering on Deuteron Target

Concerns about contamination in the HERMES target prompted an attempt to select elastic Lepton-Deuteron events. The hope was that by analyzing deuteron target data, these events could be identified, then searched for in the proton target data as evidence of contamination. The angular separation of elastic lepton-proton and lepton-deuteron events is large enough to resolve (See Figure 3.1).

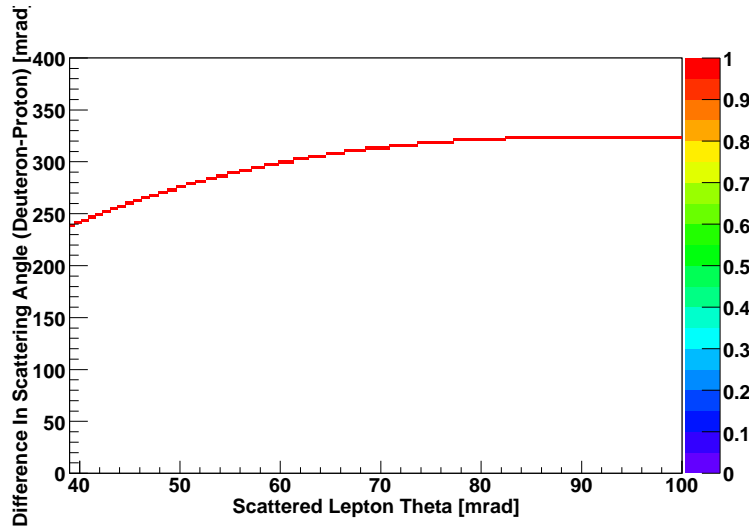


Figure 3.1: The angular difference between the scattered hadron for the two types of elastic events.

Since the distribution of the ϕ and Z-vertex differences should be the same as for the elastic proton events, these correlation cuts were made identically as before in order

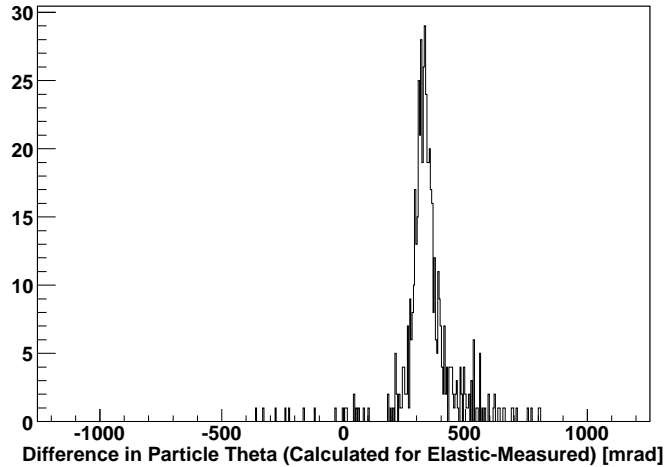


Figure 3.2: θ difference (calculated-measured) [mrad] for events from deuteron data. The calculated value is the expected scattering angle of a deuteron.

to reduce background. The θ difference was then examined to search for the elastic events. The data is seen to be dominated by the quasi-elastic lepton-proton events, as the region of Figure 3.2 in which the elastic deuteron events are expected (~ 40 – 100 mrad) shows no events. Calculation using the same methods as in 2.3.2 (assuming two body kinematics and proton scattering) gives Figure 3.3, which clearly shows that these are quasi-elastic events. At these energies, the cross section for elastic events is expected to be much smaller than that for quasi-elastic, so this result is unsurprising.

Although no signal from lepton-deuteron elastic events was observed, the dominance of quasi-elastic scattering allows comparison of the deuteron target plots with those from elastic lepton-proton events. The peaks in the θ , ϕ and Z-vertex plots for the deuteron data are at approximately the same values as those from the proton data. Peaks widths are generally greater because the events are quasi-elastic and more complicated than the simple two body collision model used in calculations. For an example of peak comparison, see Figure 3.4.

4 Detector Alignment and Efficiency

4.1 θ and ϕ Acceptance

The distribution of events in θ and ϕ for each detector was plotted. Figure 4.1 suggests that the beam is not exactly at $(0, 0)$ in the X-Y plane of the detectors. The acceptance in ϕ at a given θ is smaller in the upper Recoil Detector quadrants (2 and 3) than in

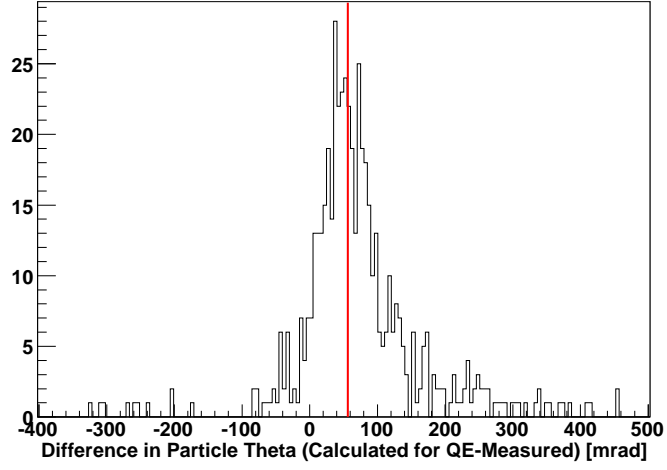


Figure 3.3: θ difference (calculated-measured) [mrad] for events in which a quasi-elastically scattered proton was detected in Quadrant 1 of the Recoil Detector. A red line indicates the mean of the peak from the correlation cut in Section 2.3.2. For simplicity, the calculation is the same as in the purely elastic proton scattering case.

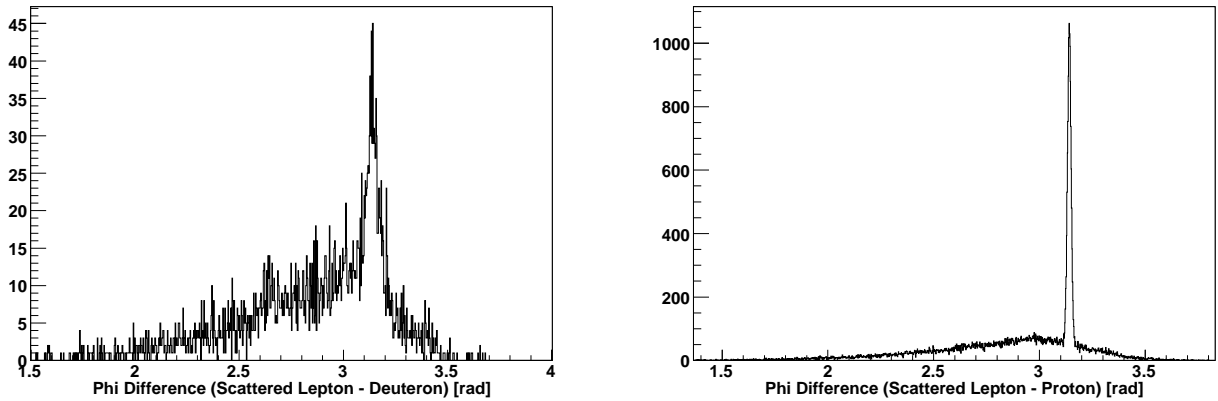


Figure 3.4: A comparison of the ϕ difference plots for deuteron data (left) and proton data (right) in Quadrant 1.

the lower quadrants (1 and 4). A similar effect is evident in the Forward Spectrometer as well.

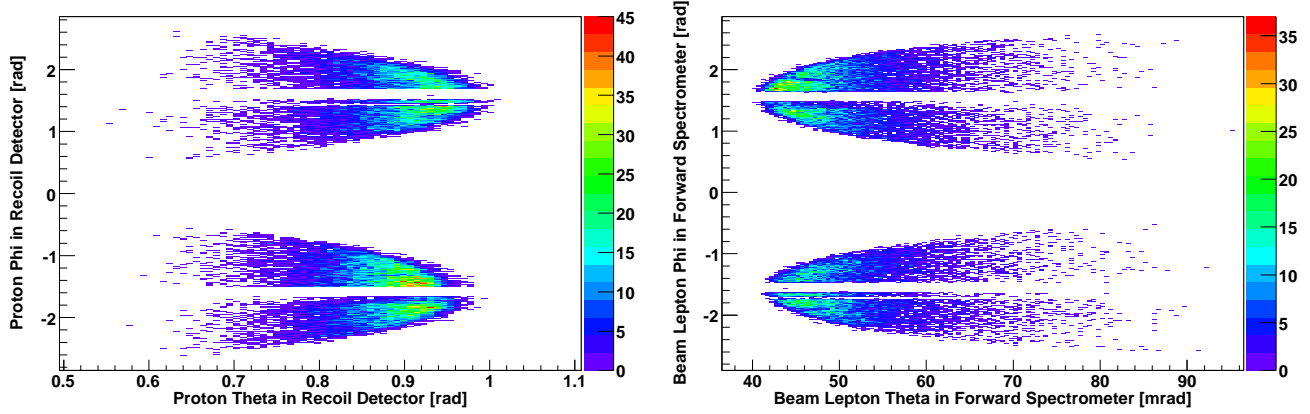


Figure 4.1: Histograms showing ϕ vs. θ for elastically scattered particles in the Recoil Detector (left) and Forward Spectrometer (right).

4.2 Z-vertex Misalignment

Significant difference in the Z-vertex position as measured by the individual detectors was evident in the fits for the correlation cuts in Section 2.3.3. The data was analyzed in order to determine whether the Recoil Detector, Forward Spectrometer, or both were at fault. Using the latest alignments, Figures 4.2 and 4.3 show a opposite and roughly equal offsets for events in the Forward Spectrometer with protons detected in Quadrants 2 and 4 of the Recoil Detector. The plot suggests a beam misalignment in the Forward Spectrometer of about 1mm along the $(1, 1)$ and negligible misalignment along $(-1, 1)$, in the X-Y plane.

4.3 Momentum Measurements

Momentum calculation in the Recoil Detector is extremely sensitive to misalignment and prone to error due to the small curvature of the high momentum proton track. The most recent alignment has significantly improved the accuracy of these calculation s. Inaccuracy is still evident, however, as can be seen in Figure 4.4 and the right plot in Figure 2.5. It should be remembered that this is an extreme regime of the Recoil Detector.

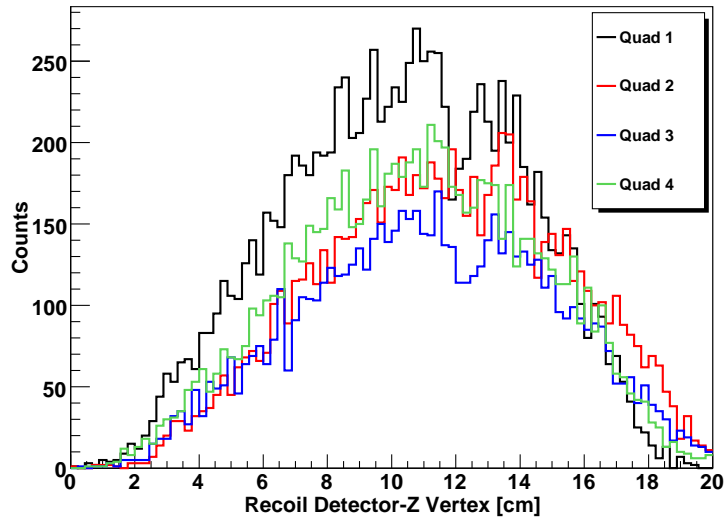


Figure 4.2: Z-Vertex distributions of elastic events in different quadrants of the Recoil Detector.

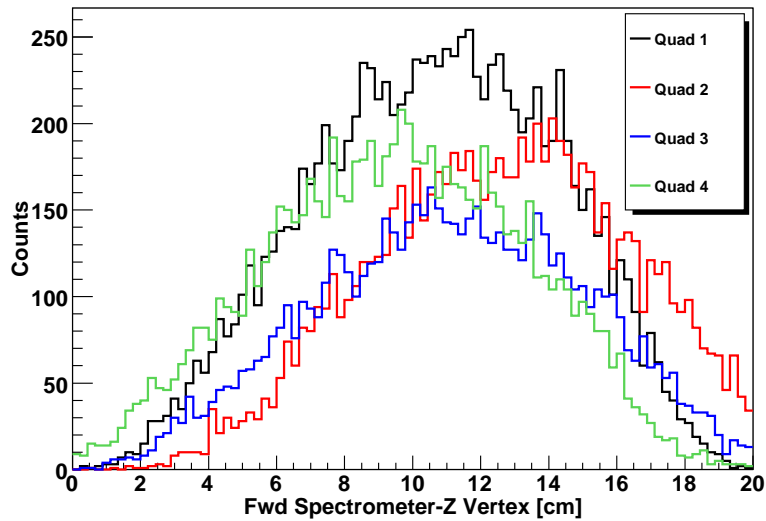


Figure 4.3: Z-Vertex distributions of elastic events as measured by the Forward Spectrometer, for events in different quadrants of the Recoil Detector.

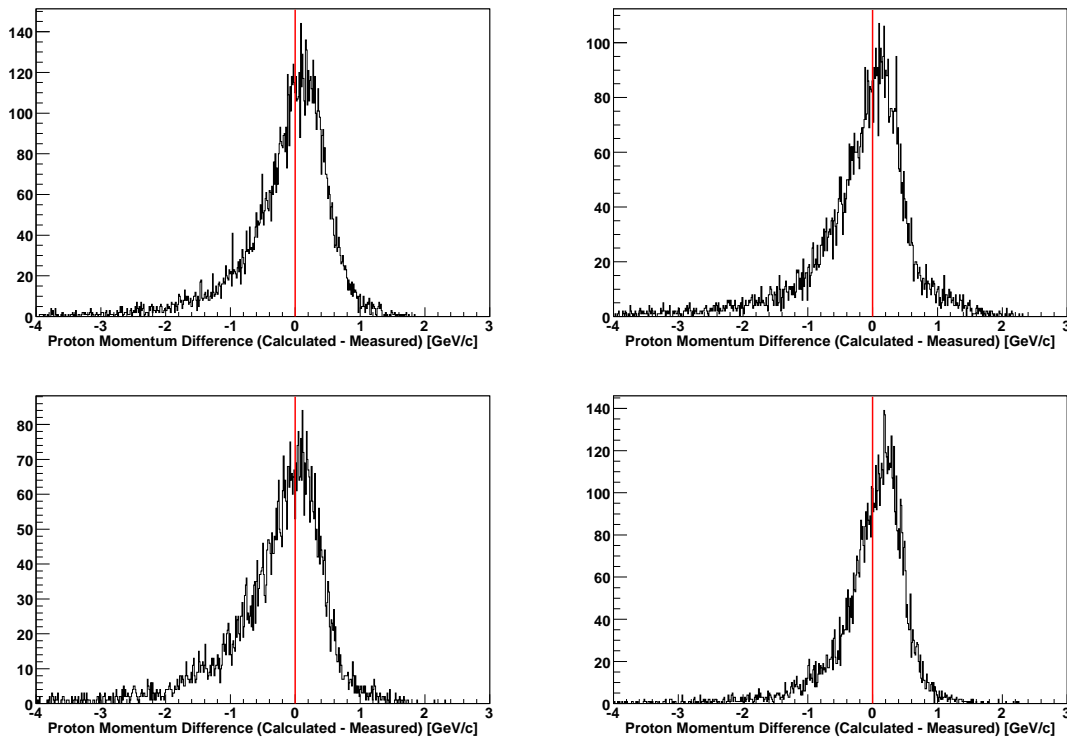


Figure 4.4: Difference of proton momentum as measured by the Recoil Detector and calculated from lepton θ for events from all quadrants.

4.4 Q^2 Distribution

One of the most important kinematic variables in HERMES analysis is Q^2 , the negative magnitude of the virtual photon's four momentum. Expression of the elastic cross section as a function of Q^2 can be used to extract the proton elastic form factors. It is calculated as

$$Q^2 \stackrel{lab}{=} 4EE' \sin^2 \left(\frac{\theta}{2} \right) \quad (4.1)$$

where E is the energy of the incoming lepton, E' is the energy of the outgoing lepton and θ is the polar angle of the same. Unfortunately, as mentioned in the introduction, luminosity and efficiency are not sufficiently well understood at this point in time and cross sections could not be computed.

An attempt was made to extract an estimate of the detector efficiency from the data. The idea was to estimate luminosity using known luminosity and DIS counts from 2006 data. This estimates was then used to normalize the Q^2 distribution. Division of this plot by the Monte Carlo Q^2 distribution, similarly normalized using the number of elastic events generated, should give an estimate of efficiency. Unfortunately, the

luminosity estimate appears to be inaccurate, as the result is an ‘estimated efficiency’ greater than one.

The shape of the Q^2 distribution itself is quite reasonable however, showing the effects of acceptance in the lower range but decaying as expected at higher values. Calculations of Q^2 using only the lepton θ and using both lepton θ and momentum are in very good agreement, which suggests good precision (Figure 4.5).

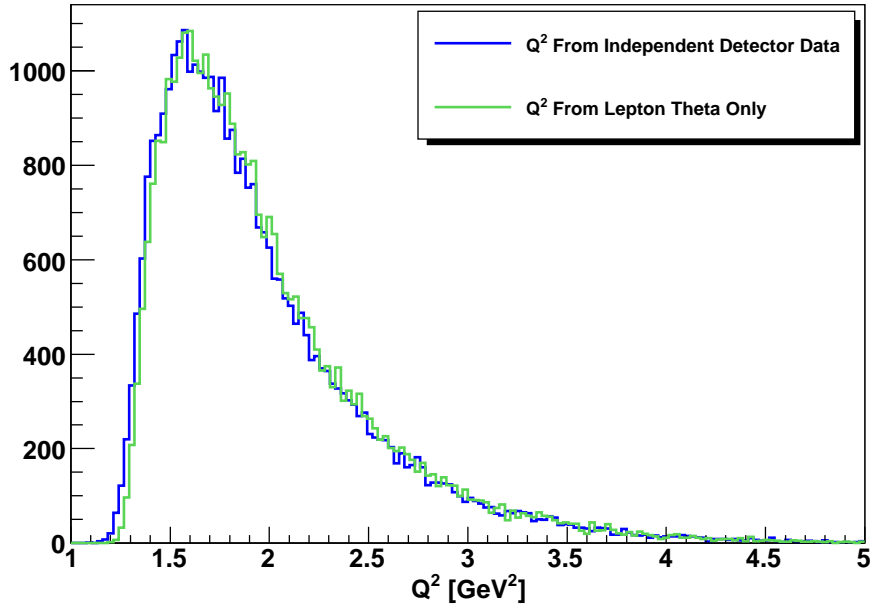


Figure 4.5: The Q^2 distribution of elastic events. In one case, independent detector variables θ_{lepton} and E'_{lepton} (the final lepton energy) are used. For the second calculation, Q^2 is calculated only from θ_{lepton} .

In Figure 4.6, the distributions from real data (using the independent variables) and Monte Carlo simulations were then both normalized to unity and plotted for comparison. They are in excellent agreement at higher Q^2 , but differences are apparent in the lower range. These differences can probably be attributed to the difference in real misalignments and the implementation of detector misalignment in the Monte Carlo simulations. This leads to differences in detector acceptance between the real and Monte Carlo data sets. In this low Q^2 region, the event count is highly sensitive to acceptance effects.

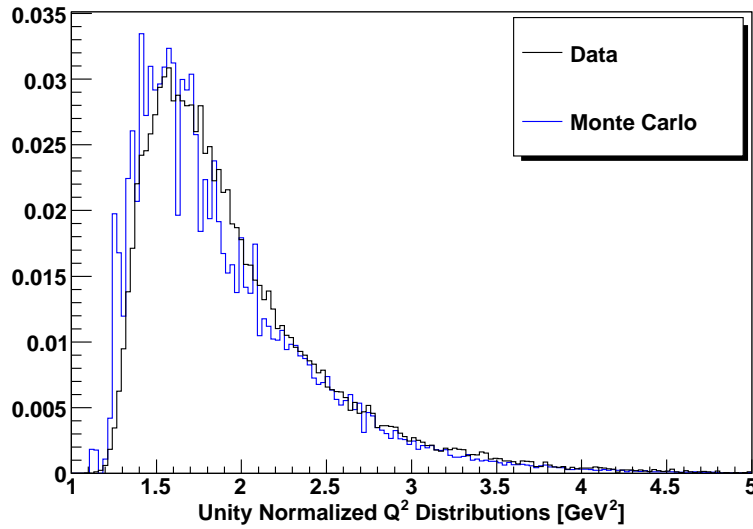


Figure 4.6: The Q^2 distributions from real and Monte Carlo data sets, normalized to unity for comparison.

5 Summary and Outlook

This study of elastic events has served to improve knowledge of the HERMES detectors, especially the Recoil Detector, and how they work together. With accurate luminosity values, the efficiency of the detector could be estimated. This would help to confirm other, more careful studies specifically intended to explore the efficiency. The work described in this report also includes a procedure for selection of elastic events, which can be used to begin calculation of the absolute cross section in the future.

Bibliography

- [1] D. Day, The Nucleon Elastic Form Factors, Nuclear Phys. A Volume 755 (2005), 151c-160c.